Heterovalent cation-substituted Aurivillius phases, $Bi_2SrNaNb_2TaO_{12}$ and $Bi_2Sr_2Nb_{3-x}M_xO_{12}$ (M = Zr, Hf, Fe, Zn)

T.K. Mandal [a], T. Sivakumar [a], S. Augustine [a], J. Gopalakrishnan [a,b,*]

[a] *Solid State and Structural Chemistry Unit, Indian Institute of Science, Bangalore 560012, India*
[b] *Jawaharlal Nehru Centre for Advanced Scientific Research, Bangalore 560064, India*

Abstract

We describe the synthesis and structural characterization of new aliovalent cation-substituted $n = 3$ Aurivillius phases of the formulas, $Bi_2SrNaNb_2TaO_{12}$ (**I**), $Bi_2Sr_2Nb_2ZrO_{12}$ (**II**), $Bi_2Sr_2Nb_{2.5}Fe_{0.5}O_{12}$ (**III**) and $Bi_2Sr_2Nb_{2.67}Zn_{0.33}O_{12}$ (**IV**). Energy dispersive X-ray (EDX) investigation of the chemical compositions showed that while cation-stoichiometric materials are formed for **I** and **II**, single-phase materials are obtained only for the compositions given for **III** and **IV** suggesting that the compositions tend to be oxygen-stoichiometric. The results show that aliovalent cation-substituted $n = 3$ Aurivillius phases similar to $Bi_2Sr_2Nb_2M^{IV}O_{12}$ (M = Ti, Mn) exist for several metal cations, viz., Ta^V, Zr^{IV}, Fe^{III} and Zn^{II}. Refinement of the crystal structures from the powder X-ray diffraction (XRD) data for **I** and **III** revealed that bismuth is essentially confined to the Bi_2O_2 layers and the aliovalent cation shows a preference for the middle perovskite sheet. The present work is significant for two reasons: firstly, the presence of cations such as Sr^{2+}, Na^+ (that do not contain lone pair s^2 electrons) in the perovskite slabs seems to render the structure centrosymmetric; secondly, a preferential/partial ordering of octahedral site cations in the perovskite slabs obtains in these materials, that seems to be dictated by a second order Jahn–Teller effect associated with d^0 cations.

Keywords: Ceramics; Oxides; Layer structures; X-ray diffraction

1. Introduction

Among the several layered variants of the perovskite structure, the Aurivillius phases, $[Bi_2O_2][A_{n-1}B_nO_{3n+1}]$, discovered [1,2] in 1949 continue to attract attention even today in view of the ferroelectric properties associated with this class of materials [3,4]. For example, $SrBi_2Ta_2O_9$ (SBT) [3] and $Bi_{3.25}La_{0.75}Ti_3O_{12}$ (BLT) [4] in thin film forms are potentially useful for non-volatile memory devices. In addition, there is current interest to develop multiferroic materials consisting of conventional "ferroelectric (d^0) cations" and "magnetic (d^n) cations". Aurivillius phases (Fig. 1) seem to be ideal candidates for this purpose. $Bi_2Sr_2Nb_2MnO_{12-\delta}$ [5] is one such material that has been synthesized recently. The structure of this material (Fig. 1b) consists of triple perovskite slabs ($Sr_2Nb_2MnO_{10-\delta}$) wherein Mn is ordered in the middle octahedral sheets and the Nb in the terminal octahedral sheets. In an effort to develop new Aurivillius phases containing different transition metal atoms in the perovskite slabs, we investigated aliovalent cation-substituted Aurivillius phases of the formula $Bi_2A_2Nb_2MO_{12-x}$, where M = Ta, Zr, Hf, Fe, Zn and A = Sr/Na. Our investigations have revealed that, whereas cation-stoichiometric phases are obtained for M = Ta and M = Zr, Hf, the phases for $M = Fe^{III}$ and $M = Zn^{II}$ tend to be cation-non-stoichiometric; single phase materials corresponding to $n = 3$ Aurivillius structure seem to obtain only for specific compositions, $Bi_2Sr_2Nb_{2.5}Fe_{0.5}O_{12}$ and $Bi_2Sr_2Nb_{2.67}Zn_{0.33}O_{12}$, that preserve anion-stoichiometry. The results of these investigations are reported in this paper.

2. Experimental

All starting materials were high purity (≥99%) chemicals obtained from Fluka except HfO_2 (∼98%). The latter was

* Corresponding author. Tel.: +91 80 2293 2537; fax: +91 80 2360 1310.
E-mail address: gopal@sscu.iisc.ernet.in (J. Gopalakrishnan).

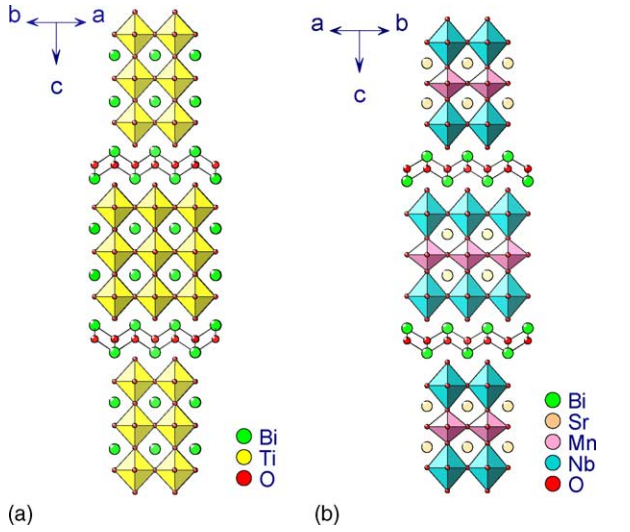

Fig. 1. Structures of typical $n = 3$ members of the Aurivillius phases: (a) $Bi_4Ti_3O_{12}$ and (b) $Bi_2Sr_2Nb_2MnO_{12-\delta}$.

obtained from BARC, Mumbai. $Bi_2SrNb_2O_9$ was prepared as reported in the literature [6] by reacting Bi_2O_3, $SrCO_3$ and Nb_2O_5 at 810 °C for 24 h and 900 °C for 24 h in air with a grinding in between. $NaTaO_3$ was prepared by reacting Na_2CO_3 and Ta_2O_5 at 600 °C for 24 h with one intermittent grinding. $Bi_2SrNaNb_2TaO_{12}$ was prepared by reacting $Bi_2SrNb_2O_9$ and $NaTaO_3$ at 1100 °C for 6 h with one intermediate grinding. $Bi_2Sr_2Nb_2MO_{12}$ (M = Zr, Hf) were prepared by reacting Bi_2O_3, $SrCO_3$ Nb_2O_5 and ZrO_2/HfO_2 at 810 °C for 24 h and 900 °C for another 24 h with intermediate grinding. For the synthesis of $Bi_2Sr_2Nb_{2.5}Fe_{0.5}O_{12}$, stoichiometric quantities of Bi_2O_3, $SrCO_3$, Nb_2O_5 and $FeC_2O_4{\cdot}2H_2O$ were thoroughly mixed and reacted at 810 °C for 24 h, 900 °C for 24 h and 1000 °C for 48 h with intermediate grindings. $Bi_2Sr_2Nb_{2.67}Zn_{0.33}O_{12}$ was made by a similar reaction of stoichiometric quantities of Bi_2O_3, $SrCO_3$, Nb_2O_5 and ZnO at 810 °C for 24 h, 900 °C for 24 h and finally at 960 °C for another 24 h with thorough intermittent grindings. The chemical compositions and synthesis conditions for the oxides prepared in this study are summarized in Table 1.

Structural characterization was made by powder X-ray diffraction (XRD) using a Siemens D5005 powder diffractometer (Cu Kα radiation). Unit cell parameters were least-squares refined by the PROSZKI [7] program. For scanning electron microscopy (SEM), samples were mounted using double-sided conducting carbon tape on brass stubs and gold-coated. Energy dispersive X-ray (EDX) analysis was carried out to determine the metal atom ratios. For this purpose, a JEOL JSM 5600 LV microscope operating in the high vacuum mode and equipped with a Link/ISIS system from Oxford Instruments was used. Powder second harmonic generation (SHG) tests were done using 1064 nm laser radiation with an equipment similar to the one described by Kurtz and Perry [8]. A pulsed Q-switched Nd:YAG laser (Spectra Physics DCR - II) with pulse duration of 8 ns was used in the experiments. Structural refinements of the powder XRD data were carried out by the Rietveld method using the XND [9] program. For structure refinements, the data were collected in the 2θ range 3°–100° with a step size of 0.02° and a step time of 9 s using Siemens D5005 X-ray powder diffractometer.

3. Results and discussion

We investigated the formation of aliovalent cation-substituted Aurivillius phases related to $Bi_2Sr_2Nb_2MO_{12}$ (M = Ti, Mn) [10,5] for M = Ta, Zr, Hf, Fe and Zn. Powder XRD pattern (Fig. 2) showed formation of a new single phase Nb/Ta compound for the composition $Bi_2SrNaNb_2TaO_{12}$ (**I**), which could be indexed on a tetragonal cell similar to $Bi_2SrNaNb_3O_{12}$ [11]. The SEM image and the corresponding EDX spectra are shown in Fig. 3 indicating that **I** is indeed a single-phase material. For M = Zr and Hf, we obtained single-phase materials for the composition $Bi_2Sr_2Nb_2MO_{12}$ (M = Zr, Hf). While the powder XRD patterns (Fig. 4) are similar to $n = 3$ Aurivillius structure; they contained additional reflections that could only be indexed on a larger tetragonal cell, where $a = b = 7.847(2)$ Å and $c = 33.854(9)$ Å. Indexed powder XRD data for Zr and Hf compounds are given in Table 2. Clearly we see a doubling of the tetragonal *a*- and *b*-axis as compared to the parent $n = 3$ Aurivillius structure. The SEM and EDX data (Fig. 5) show that both the Zr and Hf oxides are indeed single-phase materials.

In contrast, for M = Fe and Zn, we could not obtain single-phase materials for the cation-stoichiometric compositions, $Bi_2Sr_2Nb_2FeO_{12-\delta}$ and $Bi_2Sr_2Nb_2ZnO_{12-\delta}$. Powder XRD patterns (Fig. 6), however, showed the formation of an $n = 3$ Aurivillius phase together with other impurity phases. Careful examination of the SEM and EDX data revealed that the products were multiphasic (for Fe-compound

Table 1
Chemical compositions, synthesis conditions and lattice parameters of aliovalent cation-substituted Aurivillius phases related to $Bi_2Sr_2Nb_2MO_{12}$ (M = Ti, Mn)

Chemical composition	Synthesis condition[a]	Lattice parameters (Å)
$Bi_2SrNaNb_2TaO_{12}$	1100 °C/3 h; 1100 °C/3 h	Tetragonal: $a = 3.896(1)$, $c = 32.839(7)$
$Bi_2Sr_2Nb_2ZrO_{12}$	810 °C/24 h; 880 °C/24 h	Tetragonal: $a = 7.847(2)$, $c = 33.854(8)$
$Bi_2Sr_2Nb_2HfO_{12}$	810 °C/24 h; 900 °C/24 h	Tetragonal: $a = 7.838(1)$, $c = 33.724(9)$
$Bi_2Sr_2Nb_{2.5}Fe_{0.5}O_{12}$	810 °C/24 h; 900 °C/24 h; 1000 °C/48 h	Tetragonal: $a = 3.910(1)$, $c = 33.241(5)$
$Bi_2Sr_2Nb_{2.67}Zn_{0.33}O_{12}$	810 °C/24 h; 900 °C/24 h; 960 °C/24 h	Orthorhombic: $a = 5.528(2)$, $b = 5.535(1)$, $c = 33.515(9)$

[a] Constituent oxides and $SrCO_3$ ($FeC_2O_4{\cdot}2H_2O$ and Na_2CO_3 where required) taken in stoichiometric proportion were reacted at the synthesis condition given. For $Bi_2SrNaNb_2TaO_{12}$, $Bi_2SrNb_2O_9$ and $NaTaO_3$ prepared separately were reacted at the synthesis condition.

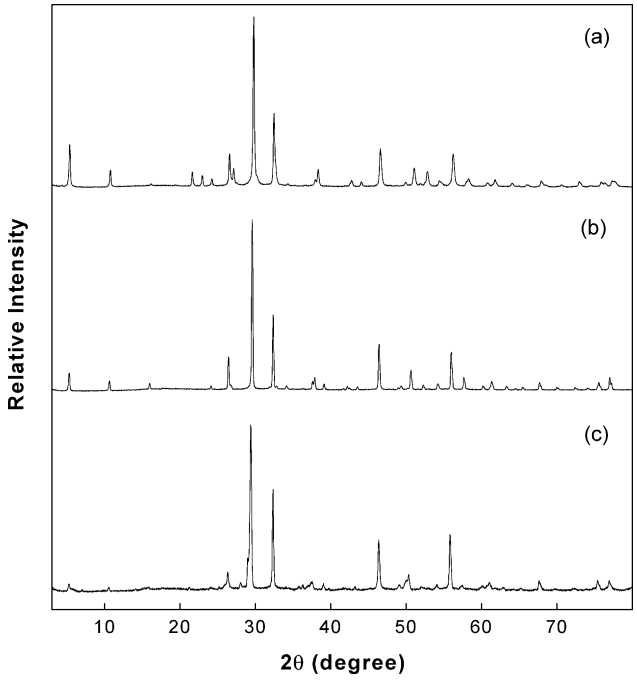

Fig. 2. Powder XRD patterns of (a) $Bi_2SrNaNb_2TaO_{12}$, (b) $Bi_2Sr_2Nb_{2.5}Fe_{0.5}O_{12}$ and (c) $Bi_2Sr_2Nb_{2.67}Zn_{0.33}O_{12}$.

the data are shown in Fig. 7). The approximate compositions of the Aurivillius phases for M = Fe and Zn estimated from EDX data are, respectively, $Bi_2Sr_2Nb_{2.5}Fe_{0.5}O_{12}$ and $Bi_2Sr_2Nb_{2.67}Zn_{0.33}O_{12}$, suggesting that the phases tend to be

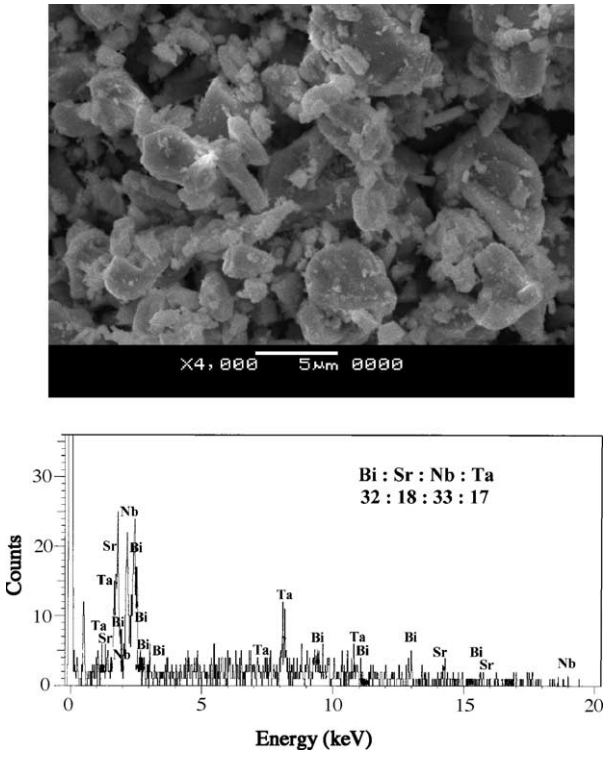

Fig. 3. SEM image and EDX spectra of $Bi_2SrNaNb_2TaO_{12}$.

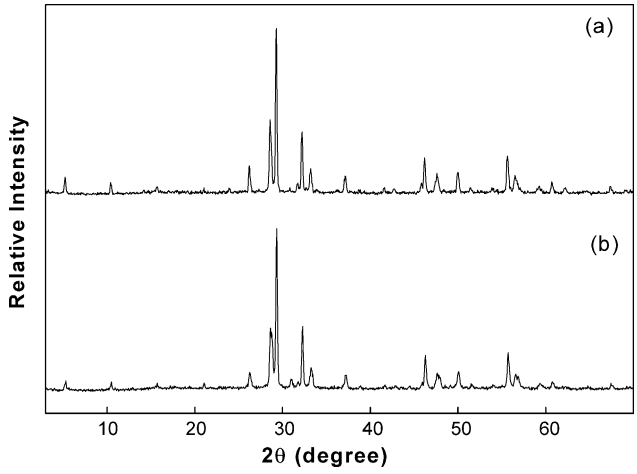

Fig. 4. Powder XRD patterns of (a) $Bi_2Sr_2Nb_2ZrO_{12}$ and (b) $Bi_2Sr_2Nb_2HfO_{12}$.

oxygen-stoichiometric. We then prepared single-phase $n = 3$ Aurivillius oxides for these compositions. SEM and EDX data (Fig. 8) confirmed that the products obtained for these compositions are single-phase materials. Their powder XRD patterns (Fig. 2b and c) could be indexed on tetragonal and orthorhombic Aurivillius structures (Table 1). The details of synthesis conditions and the lattice parameters of the aliovalent cation-substituted $n = 3$ Aurivillius phases synthesized in this study are summarized in Table 1.

We have determined the crystal structures of two representative members namely, $Bi_2SrNaNb_2TaO_{12}$ (**I**) and $Bi_2Sr_2Nb_{2.5}Fe_{0.5}O_{12}$ (**III**), by Rietveld refinement of powder XRD data using the XND [9] program. The starting model for the refinement of the structure of $Bi_2SrNaNb_2TaO_{12}$ (**I**) was constructed using the atomic coordinates of $Bi_2SrNaNb_3O_{12}$ [11] (*I*4/*mmm* space group) wherein the Nb(1) (2a site) in the central perovskite layer is replaced by Ta. For this ideal model, where the TaO_6 octahedra are flanked by NbO_6 octahedra in the triple-layered perovskite slab, we find that one of the oxygen positions, O4, is refined to an unrealistic value (0, 0, ∼0.12). However, when we allowed random mixing of the Ta and Nb sites (2a and 4e sites, respectively), the refinement yielded reasonable oxygen position (0, 0, ∼0.06). Subsequently, we have refined the occupancies of Nb and Ta in their respective sites. We have also allowed the mixing of Sr^{2+} in the perovskite site and Bi^{3+} in $[Bi_2O_2]$ layer and found that ∼7% of Sr^{2+} are disordered into the $[Bi_2O_2]$ layer. (We have not allowed mixing of A-site Na in the $[Bi_2O_2]$ layer since this is quite unlikely.) The refined atomic coordinates, occupancies, isotropic temperature factors (B_{iso}) are listed in Table 3 and selected bond distances along with bond valence sums (BVSs) in Table 4. The Rietveld profile fit is shown in Fig. 9. In Fig. 10, we show the crystal structure of **I** drawn from the coordinates given in Table 3. The refinement shows that **I** adopts a typical $n = 3$ Aurivillius layered perovskite structure, consisting of triple-layered perovskite slabs, $[SrNaNb_2TaO_{10}]$, interleaved by $[Bi_2O_2]$ sheets. The

Table 2
X-ray powder diffraction data for $Bi_2Sr_2Nb_2ZrO_{12}$ and $Bi_2Sr_2Nb_2HfO_{12}$

$Bi_2Sr_2Nb_2ZrO_{12}$[a]						$Bi_2Sr_2Nb_2HfO_{12}$[b]					
h	*k*	*l*	d_{obs} (Å)	d_{calc} (Å)	I_{obs}	*h*	*k*	*l*	d_{obs} (Å)	d_{calc} (Å)	I_{obs}
0	0	4	8.431	8.464	6	0	0	2	16.79	16.86	8
0	0	6	5.630	5.642	4	0	0	4	8.421	8.431	6
0	0	8	4.220	4.232	2	0	0	6	5.637	5.621	3
2	0	3	3.710	3.706	2	0	0	8	4.214	4.216	4
1	0	9	3.389	3.392	16	1	0	9	3.386	3.381	12
2	1	5	3.119	3.116	44	2	1	5	3.112	3.110	35
2	0	7	3.048	3.047	100	2	0	7	3.042	3.040	100
1	1	10	2.900	2.890	2	1	1	10	2.879	2.881	6
0	0	12	2.824	2.821	5	0	0	12	2.813	2.810	3
2	2	0	2.778	2.774	36	2	2	0	2.771	2.771	36
2	1	8	2.700	2.701	14	2	1	8	2.693	2.695	14
2	0	11	2.421	2.422	12	2	0	11	2.413	2.415	12
3	2	1	2.173	2.172	3	2	2	8	2.316	2.316	3
0	0	16	2.117	2.116	2	3	2	1	2.165	2.169	2
2	2	12	1.979	1.978	6	0	0	16	2.108	2.108	3
4	0	0	1.962	1.962	21	1	0	16	2.035	2.035	3
4	0	4	1.909	1.911	11	4	0	0	1.959	1.959	23
2	2	14	1.824	1.823	12	4	0	4	1.908	1.909	12
2	0	17	1.776	1.776	3	4	1	1	1.898	1.898	11
4	2	5	1.699	1.698	3	2	2	14	1.820	1.818	13
4	0	11	1.652	1.654	23	2	0	17	1.773	1.773	4
3	3	10	1.627	1.623	9	4	2	5	1.697	1.696	3
4	2	10	1.557	1.558	5	4	0	11	1.648	1.651	25
4	0	14	1.524	1.523	7	3	3	10	1.625	1.620	9
4	3	7	1.492	1.493	4	4	2	8	1.618	1.618	8
1	0	24	1.388	1.388	5	4	2	10	1.554	1.555	4
						4	0	14	1.522	1.520	6
						4	4	0	1.386	1.385	4

[a] $a = 7.847(2)$ Å, $b = 7.847(2)$ Å and $c = 33.854(9)$ Å.
[b] $a = 7.838(1)$ Å, $b = 7.838(1)$ Å and $c = 33.724(9)$ Å.

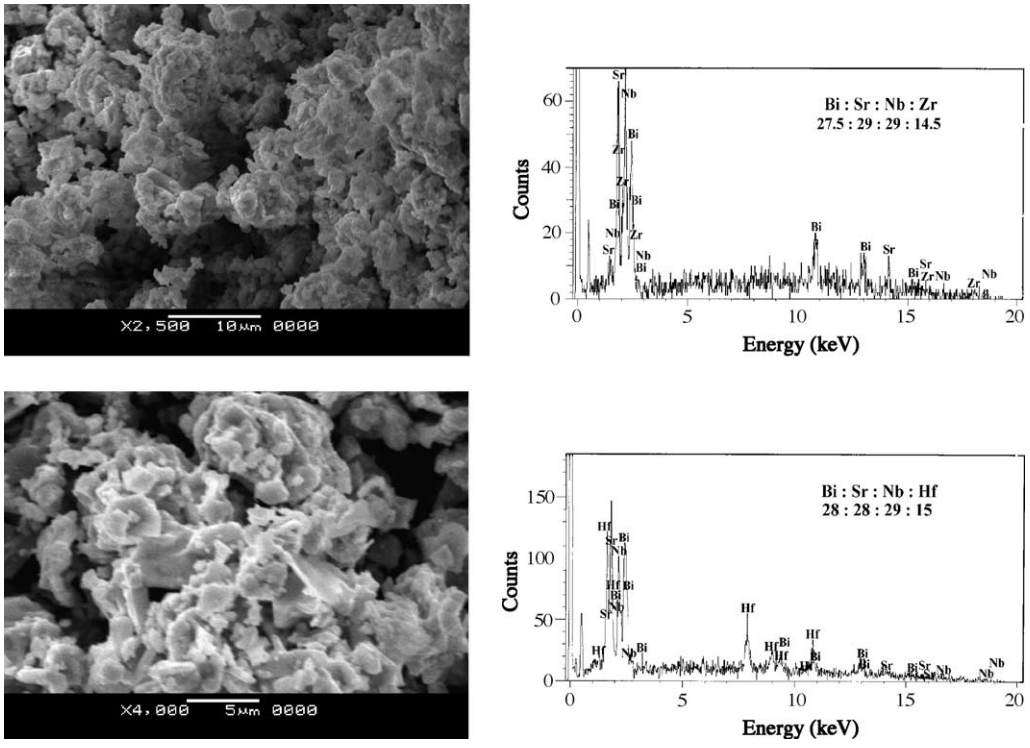

Fig. 5. SEM images of $Bi_2Sr_2Nb_2ZrO_{12}$ (top) and $Bi_2Sr_2Nb_2HfO_{12}$ (bottom). The right side panel shows the corresponding EDX spectra.

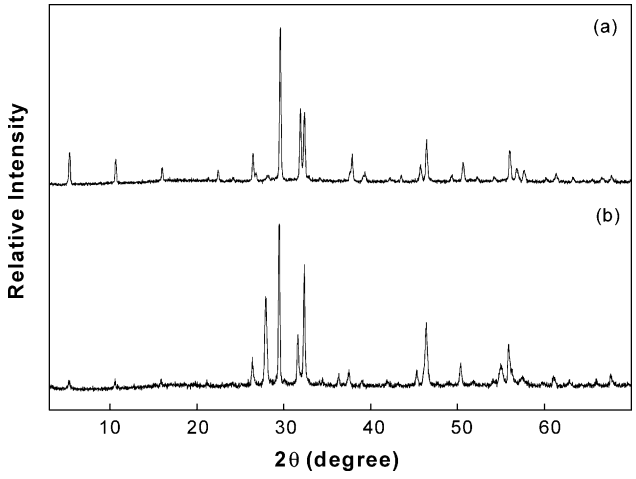

Fig. 6. Powder XRD patterns of nominal (a) $Bi_2Sr_2Nb_2FeO_{12-\delta}$ and (b) $Bi_2Sr_2Nb_2ZnO_{12-\delta}$.

refinement also shows that the extent of disorder between Sr^{2+} in the perovskite A-site and Bi^{3+} in the $[Bi_2O_2]$ layer is only about 7%, whereas within the perovskite slab, the M2 sites (terminal octahedra) are preferentially occupied by Nb (Nb/Ta: 74/26) and the M1 site (central octahedra) by Nb/Ta (Nb/Ta: 52/48). A similar distribution of cations between M1 and M2 sites has been reported for $Bi_2Sr_2Nb_2TiO_{12}$ [10].

The Nb/TaO_6 octahedra in the triple-perovskite slabs (Fig. 10b) show the characteristic distortion arising from the second order Jahn–Teller (SOJT) effect associated with the d^0 cations [12–14]. The distortion parameter, Δ, defined as, $\Delta = 1/n\Sigma\{(r_i - r)/r\}^2 \times 10^3$ [15], for the central Ta/NbO_6 and terminal Nb/TaO_6 octahedra is 0.035 and 5.415, respectively, indicating that the terminal octahedra are more distorted as compared to the central one. Similar

Table 3
Atomic coordinates, isotropic temperature factors and occupancies for $Bi_2SrNaNb_2TaO_{12}$

Atom	Site	Occupancy	x	y	z	B_{iso} (Å^2)
Bi[a]	4e	0.93	0.0	0.0	0.2868(1)	4.8(1)
Sr[a]	4e	0.07	0.0	0.0	0.2868(1)	4.8(1)
Bi[b]	4e	0.07	0.0	0.0	0.4359(2)	2.8(1)
Sr[b]	4e	0.43	0.0	0.0	0.4359(2)	2.8(1)
Na[b]	4e	0.50	0.0	0.0	0.4359(2)	2.8(1)
Ta1	2a[c]	0.48	0.0	0.0	0.0	2.3(1)
Nb1	2a[c]	0.52	0.0	0.0	0.0	2.3(1)
Ta2	4e[d]	0.26	0.0	0.0	0.1255(1)	1.6(1)
Nb2	4e[d]	0.74	0.0	0.0	0.1255(1)	1.6(1)
O1	4d	1.0	0.0	0.5	0.25	5.3(8)
O2	4c	1.0	0.0	0.5	0.0	3.4(7)
O3	8g	1.0	0.0	0.5	0.1150(5)	5.5(6)
O4	4e	1.0	0.0	0.0	0.0582(5)	2.1(6)
O5	4c	1.0	0.0	0.0	0.1780(6)	4.2(8)
Space group	*I*4/*mmm*					
a	3.8992(2) Å					
c	32.877(3) Å					

[a] Cation site in Bi_2O_2 layer.
[b] A-cation site in the perovskite layer.
[c] M1 site in the perovskite slab.
[d] M2 site in the perovskite slab (Fig. 10).

Table 4
Selected bond distances (Å) and bond valence sums (BVSs) for $Bi_2SrNaNb_2TaO_{12}$

Nb2/Ta2–O5	1.73(2)
Nb2/Ta2–O4	2.21(2)
Nb2/Ta2–O3 (×4)	1.980(1)
Ta1/Nb1–O4 (×2)	1.91(2)
Ta1/Nb1–O2 (×4)	1.950(1)
Average BVSs	
Central Ta/Nb	5.56
Terminal Nb/Ta	5.31

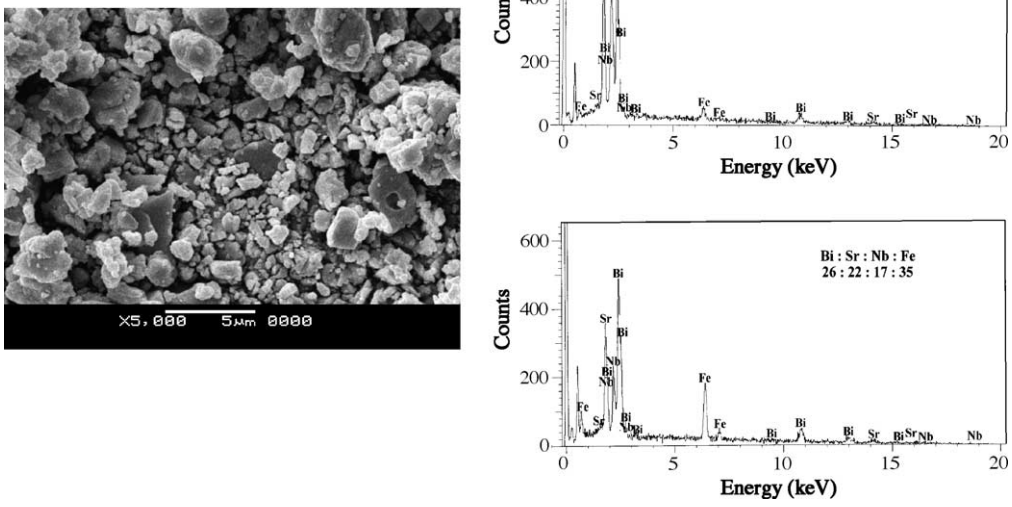

Fig. 7. SEM image and EDX spectra for nominal $Bi_2Sr_2Nb_2FeO_{12-\delta}$, showing multiphases.

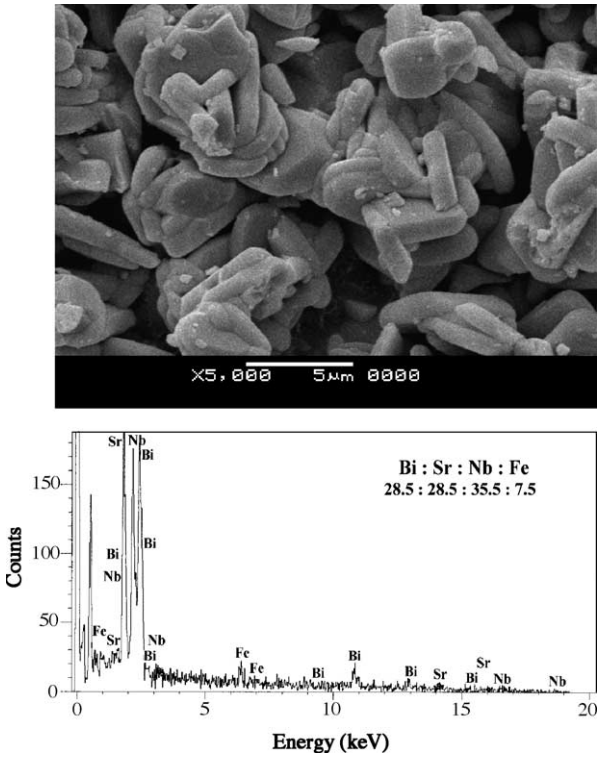

Fig. 8. SEM image and EDX spectra for $Bi_2Sr_2Nb_{2.5}Fe_{0.5}O_{12}$.

distortion parameters have been reported for other layered perovskites [15].

For refinement of the structure of $Bi_2Sr_2Nb_{2.5}Fe_{0.5}O_{12}$ (**III**), the initial model was constructed using the atomic coordinates of $Bi_2Sr_2Nb_2MnO_{12-\delta}$ [5] (space group *Fmmm*) wherein Mn^{4+} (4b site) is replaced by 50% of Nb^{5+} and 50% of Fe^{3+}, keeping the oxygen (O1; 8e site) site fully occupied. The *R*-factors R_{wp}, R_p and R_{Bragg} converged to 7.39, 5.05 and 9.58%, respectively, and the lattice parameters are $a = 5.532(5)$ Å, $b = 5.531(5)$ Å and $c = 33.266(4)$ Å. However, in the refinement of isotropic temperature factors

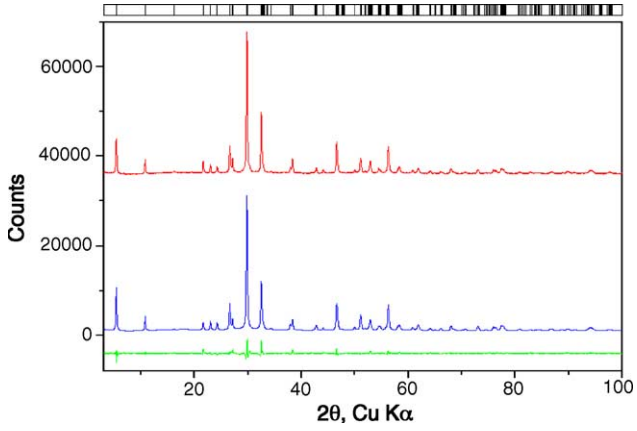

Fig. 9. Observed (top), Rietveld refined (middle) and difference (bottom) XRD profiles of $Bi_2SrNaNb_2TaO_{12}$. Vertical lines on the top panel above the figure indicate the expected Bragg reflections for the space group *I*4/*mmm*.

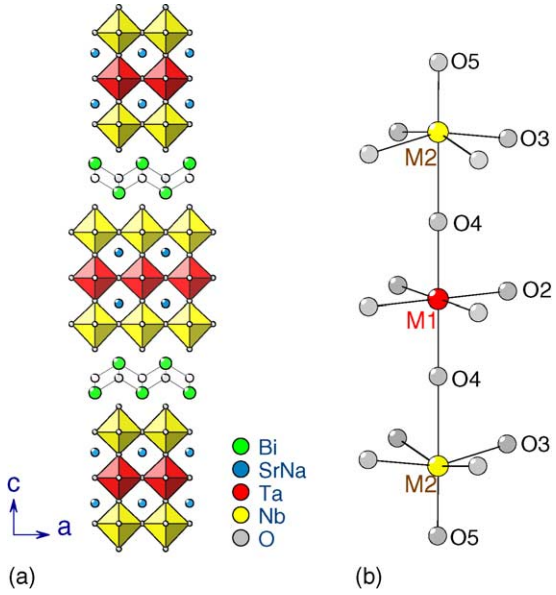

Fig. 10. (a) Structure of $Bi_2SrNaNb_2TaO_{12}$ and (b) shows the Nb/TaO_6 octahedra in the structure.

(B_{iso}), we noticed that the B_{iso} for Bi (8i site) was high [3.3(1) Å^2], indicating that the Bi site could be disordered. Therefore, we allowed mixing of Sr^{2+} in the perovskite layer and Bi^{3+} in the (Bi_2O_2). The refinement yielded similar *R*-factors ($R_{wp} = 7.20\%$ and $R_p = 4.98\%$), but the B_{iso} for Bi in (Bi_2O_2) layer remained unaffected [3.3(1) Å^2] and the lattice parameters converged to $a = 5.53(4)$ Å, $b = 5.53(4)$ Å and $c = 33.266(4)$ Å, suggesting that the compound could be tetragonal instead of orthorhombic. Moreover, the refinement of O1 occupancy (with fixed B_{iso} at 1.5 Å^2) showed that the site is fully occupied corresponding to the oxygen-stoichiometric formula $Bi_2Sr_2Nb_{2.5}Fe_{0.5}O_{12}$ (**III**). We could, however, refine the structure of **III** successfully using the atomic coordinates of $Bi_2Sr_2Nb_2TiO_{12}$ [10] with tetragonal *I*4/*mmm* space group. Observed, calculated and difference profiles for the stable refinement are shown in Fig. 11. The

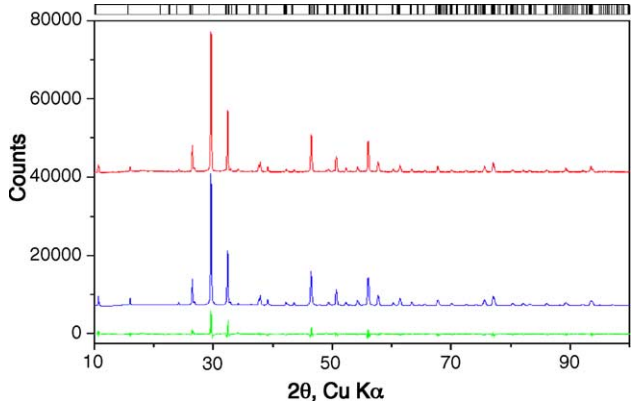

Fig. 11. Observed (top), Rietveld refined (middle) and difference (bottom) XRD profiles of $Bi_2Sr_2Nb_{2.5}Fe_{0.5}O_{12}$. Vertical lines on the top panel above the figure indicate the expected Bragg reflections for the space group *I*4/*mmm*.

Table 5
Atomic coordinates, isotropic temperature factors and occupancies for $Bi_2Sr_2Nb_{2.5}Fe_{0.5}O_{12}$

Atom	Site	Occupancy	x	y	z	B_{iso} (Å^2)
Bi[a]	4e	0.85	0.0	0.0	0.2139(1)	1.6(1)
Sr[a]	4e	0.15	0.0	0.0	0.194(1)	1.6(1)
Bi[b]	4e	0.15	0.0	0.0	0.0630(1)	1.7(1)
Sr[b]	4e	0.85	0.0	0.0	0.0630(1)	1.7(1)
Fe1	2b[c]	0.50	0.0	0.0	0.5	1.6(2)
Nb1	2b[c]	0.50	0.0	0.0	0.5	1.6(2)
Nb2	4e[d]	1.0	0.0	0.0	0.3734(1)	1.9(1)
O1	4c	1.0	0.0	0.5	0.0	1.6(3)
O2	4d	1.0	0.0	0.5	0.25	1.6(3)
O3	4e	1.0	0.0	0.0	0.4414(7)	1.6(3)
O4	4e	1.0	0.0	0.0	0.3180(8)	1.6(3)
O5	8g	1.0	0.0	0.5	0.1179(6)	1.6(3)
Space group	*I*4/*mmm*					
a	3.9109(3) Å					
c	33.257(3) Å					

[a] Cation site in Bi_2O_2 layer.
[b] A-cation site in the perovskite layer.
[c] M1 site in the perovskite slab.
[d] M2 site in the perovskite slab.

atomic positions, occupancies, thermal parameters are listed in Table 5. Selected bond lengths and bond valence sums are given in Table 6. We obtained reasonable B_{iso} values (Table 5) for all the atoms including Bi^{3+} in the (Bi_2O_2) layer with ~15% cation disorder between perovskite A-site (Sr^{2+}) and the Bi^{3+} site in the (Bi_2O_2) layer. A significant feature of the refinement is that Fe^{3+} is essentially confined to the middle octahedral layer in the triple perovskite sheet (M1 site is occupied by $Fe_{0.5}Nb_{0.5}$). The terminal M2 sites in the perovskite sheet are exclusively occupied by Nb. Bond valence sums are consistent with the expected oxidation states. In Fig. 12, we show the crystal structure of **III** drawn from the coordinates given in Table 5. The NbO_6 and Nb/FeO_6 octahedra in the structure are shown in Fig. 12b. Here again, we see that the terminal NbO_6 octahedra are significantly distorted ($\Delta = 3.565$) as compared to the central Fe/NbO_6 octahedra ($\Delta = 0.002$).

All the Aurivillius phases described herein are SHG inactive towards 1064 nm laser radiation. The result is consistent with the centrosymmetric structure as evident from the powder XRD data. Interestingly, $Bi_2Sr_2Nb_2MnO_{12-\delta}$ (*Fmmm*) and $Bi_2Sr_2Nb_2TiO_{12}$ (*I*4/*mmm*) also adopt centrosymmetric structures. As compared to the parent $n = 3$ Aurivillius phase,

Table 6
Selected bond distances (Å) and bond valence sums (BVSs) for $Bi_2Sr_2Nb_{2.5}Fe_{0.5}O_{12}$

Nb2–O4	1.84(3)
Nb2–O5	2.26(2)
Nb2–O3 (×4)	1.977(3)
Fe1/Nb1–O3 (×2)	1.950(2)
Fe1/Nb1–O1 (×4)	1.955(1)
Average BVSs	
Central Nb/Fe	4.372
Terminal Nb	4.948

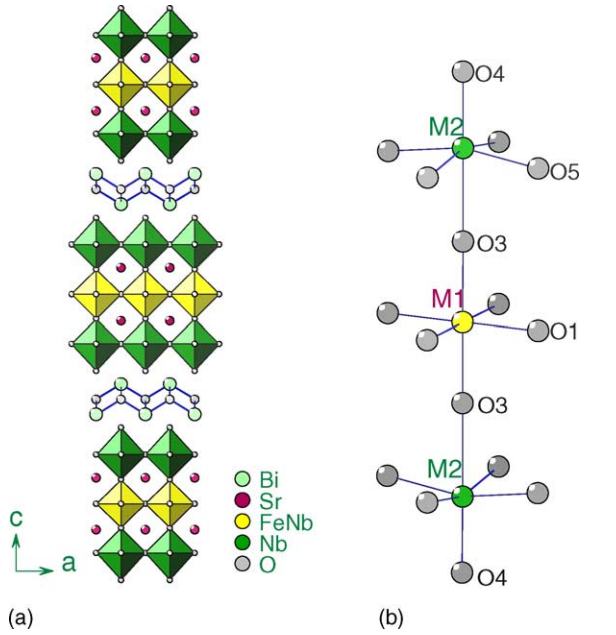

Fig. 12. (a) Structure of $Bi_2Sr_2Nb_{2.5}Fe_{0.5}O_{12}$ and (b) shows the NbO_6 and Nb/FeO_6 octahedra in the structure.

$Bi_4Ti_3O_{12}$, which is non-centrosymmetric (*B*2*cb*) and ferroelectric, the loss of centrosymmetry in the present series of compounds is significant. This is probably related to the presence of non-s^2 Sr^{2+} in the perovskite slabs. A similar loss of centrosymmetry is observed for $Bi_2La_2Ti_3O_{12}$ [16,17], where La^{3+} occupies the perovskite slabs.

4. Conclusions

The present work shows the flexibility of the Aurivillius structures $[Bi_2O_2][A_{n-1}B_nO_{3n+1}]$ for substitution of aliovalent/isovalent cations at both A and B sites of the perovskite slabs. For example, in a typical $n = 3$ member, $Bi_2Sr_2Nb_2TiO_{12}$, substitution of both Sr and Na at the A site and Ta at the B site has enabled us to synthesize a new $n = 3$ member, $Bi_2SrNaNb_2TaO_{12}$, where we see a preference of Nb for the terminal octahedral sheets. Similarly, aliovalent substitution only at the B site of the perovskite slabs of $Bi_2Sr_2Nb_2TiO_{12}$ has yielded new members for specific compositions, $Bi_2Sr_2Nb_2ZrO_{12}$, $Bi_2Sr_2Nb_{2.5}Fe_{0.5}O_{12}$ and $Bi_2Sr_2Nb_{2.67}Zn_{0.33}O_{12}$ that tend to be oxygen-stoichiometric. The latter phases again show a preference for Nb for the terminal octahedral sites that are strongly distorted as compared to the middle octahedral site.

Acknowledgement

We thank the Department of Science and Technology, Government of India, New Delhi, for support of this work.

References

[1] B. Aurivillius, Ark. Kemi 1 (1949) 463.
[2] B. Aurivillius, Ark. Kemi 2 (1950) 519.
[3] C.A. Paz de Araujo, J.D. Cuchiaro, L.D. Mcmallian, M.C. Scott, J.F. Scott, Nature 374 (1995) 627.
[4] B.H. Park, B.S. Kang, S.D. Bu, T.W. Noh, J. Lee, W. Jo, Nature 401 (1999) 682.
[5] W.J. Yu, Y.I. Kim, D.H. Ha, J.H. Lee, Y.K. Park, S. Seong, N.H. Hur, Solid State Commun. 111 (1999) 705, A recent paper, E.E. McCabe, C. Greaves, J. Mater. Chem. 15 (2005) 177, describes the formation of $Bi_2Sr_{1.4}La_{0.6}Nb_2MnO_{12}$ instead of $Bi_2Sr_2Nb_2MnO_{12}$.
[6] Ismunandar, B.J. Kennedy, Gunawan, Marsongkohadi, J. Solid State Chem. 126 (1996) 135.
[7] W. Losocha, K. Lewinski, J. Appl. Crystallogr. 27 (1994) 437.
[8] S.K. Kurtz, T.T. Perry, J. Appl. Phys. 39 (1968) 3798.
[9] J.-F. Bérar, Program XND, ESRF, Grenoble, France (More information under: http://www.ccp14.ac.uk);
J.-F. Bérar, Proceedings of the IUCr Satellite Meeting on Powder Diffractometry, Toulouse, France, July 1990;
J.-F. Bérar, P. Garnier, II APD Conference, NIST (USA), Gaithersburg, MD, May 1992;
J.-F. Bérar, P. Garnier, NIST Spec. Publ. 846 (1992) 212.
[10] M.S. Heluska, S.T. Misture, J. Solid State Chem. 177 (2004) 1965.
[11] W. Sugimoto, M. Shirata, K. Kuroda, Y. Sugahara, Chem. Mater. 14 (2002) 2946.
[12] N.S.P. Bhuvanesh, J. Gopalakrishnan, J. Mater. Chem. 7 (1997) 2297.
[13] R.A. Wheeler, M.H. Whangbo, T. Hughbanks, R. Hoffmann, J.K. Burdett, T.A. Albright, J. Am. Chem. Soc. 108 (1986) 2222.
[14] S.K. Kang, H. Tang, T.A. Albright, J. Am. Chem. Soc. 115 (1993) 1971.
[15] R.H. Mitchell, Perovskites: Modern and Ancient, Almaz Press, Thunder Bay, Canada, 2002.
[16] J. Gopalakrishnan, T. Sivakumar, K. Ramesha, V. Thangadurai, G.N. Subbanna, J. Am. Chem. Soc. 122 (2000) 6237.
[17] N.C. Hyatt, J.A. Hriljac, T.P. Comyn, Mater. Res. Bull. 38 (2003) 837.